

Investigation of ionospheric and geomagnetic response during 2011 Tohoku earthquake using ground based measurement

Norbaizura Yaso^{a*}, Alina Marie Hasbi^{a,b} & Mardina Abdullah^{a,b}

^aSpace Science Center (ANGKASA), Institute of Climate Change, Universiti Kebangsaan Malaysia, Malaysia

^bDepartment of Electrical, Electronic and Systems Engineering, Faculty of Engineering and Built Environment, Universiti Kebangsaan Malaysia

Received 7 May 2015; revised 29 July 2016; accepted 26 August 2016

This paper investigates co-seismic ionospheric disturbances (CID) during the M9.0, 11 March 2011 Tohoku earthquake. The investigation collects data from two sources which are GPS-TEC from GEONET data network and the geomagnetic field from MAGDAS data network. Three types of CID have been detected: direct acoustic wave (894m/s), secondary wave from the Rayleigh surface wave (2862 m/s), and gravity wave from a propagating Tsunami (226 m/s). The directivity of wave propagation has been found to be northward from the epicenter. Short period CID corresponding to direct acoustic waves have been firstly found about 7 min after the main shock and ended 38 min after the main shock with oscillation period varying from 2-7 min. The long period of CID corresponding to Tsunami waves firstly observed 20 min after the main shock, with 10 min of oscillation period and duration of 60 min. Geomagnetic field disturbances have been detected 10-11 min after the main shock with period of 4 min. These geomagnetic field disturbances have been associated with the short-period CID induced by the direct acoustic wave from the epicenter. The correlation between the ionospheric and geomagnetic disturbance shows a good agreement in wave characteristic.

Keywords: GPS-TEC, Geomagnetic field, Co-seismic ionospheric disturbance (CID), Tsunami

1 Introduction

Giant earthquakes that occur in the subduction zones around the world cause tsunamis and significant catastrophic damage especially in the coastal areas of many countries. The 2004 Sumatran-Andaman earthquake located in the Indian Ocean caused a subsequent tsunami in 13 countries in South Asia and East Africa with major damages where more than 297,248 lives were lost and economic losses exceeding \$10 billion. The 2010 Chile earthquake killed 521 people and estimates of economic damage were around \$30 billion. The Tohoku 2011 earthquake triggered a giant tsunami and caused an extensive damage on the coastal area, especially in the northeast of Japan. The earthquake claimed the lives of 15,854 victims in Japan while another 3,023 victims were missing. The earthquake and tsunami caused over \$200 billion worth of damages in Japan and resulted in a nuclear accident. This earthquake is the fourth largest in the world and the largest in Japan since instrumental recording began in 1990 (<http://www.ngdc.noaa.gov>). This tragedy has initiated an international society to

construct a global tsunami warning system, which involves seismic and sea level monitoring instruments¹. However, tsunami is still difficult to predict. Therefore, it is vital that the mechanism of tsunami is understood and close investigation on ways to reduce damages of future tsunami threats is carried out². The monitoring of earthquakes gives good estimation of the potential tsunamis generated by identifying the location and characteristics of the earthquake.

Ionospheric disturbances during earthquakes were firstly reported by using Doppler and ionosonde sounding^{3,4}. Nowadays, GPS technology is currently being used to measure the changes that occur to the total electron content (TEC) in the ionosphere that are triggered by seismic activities and tsunami waves⁵⁻⁹. The ionospheric disturbances, that are observed during earthquakes, are known as co-seismic ionospheric disturbance (CID). CID can be categorized into three types which are (i) direct acoustic wave from the epicenter with velocity of 700-1200 m/s and period of 4-5 min. Their waveforms have been described as 'N-type'¹⁰; (ii) secondary acoustic wave excited in areas away from the epicenter by Rayleigh surface wave with velocity 3500 m/s and period of 3-4 min; (iii) gravity wave from the focal area or

*Corresponding author (E-mail: norbaizura.yaso@gmail.com)

from propagating tsunami with velocity of 200-250 m/s and period of 10-20 min¹¹ and describe as W-type. Short period CID induced by direct acoustic wave was reported during the 2004 Sumatra-Andaman earthquake^{4,12}, the 2005 Sumatra-Andaman earthquake¹³, the 2003 Tokachi-Oki earthquake⁴ and the recent 2011 Tohoku earthquake^{14,15}. The CID was observed at about 11 min following the large earthquakes and had periods of 4-5 min. Rayleigh waves were detected during the 2004 Sumatra-Andaman earthquake^{11,12,16} and the March 2011 Tohoku earthquake^{9,15,17,18}. Meanwhile, long period disturbances induced by the tsunami were observed during the 2004 Sumatra-Andaman earthquake^{4,12} the 2001 Peru earthquake using GPS TEC measurements⁷ while the 2011 Tohoku earthquake was detected by ionosondes¹⁷ and GPS TEC¹⁹.

Shinagawa²⁰ developed a numerical simulation model to investigate the ionospheric and atmospheric variations during the occurrence of the 26 December 2004 Sumatra-Andaman earthquake. They found that the disturbance in the lower atmosphere created by the movements of the sea surface due to the earthquake event produced vertically propagating acoustic waves that also perturbed the ionosphere²⁰. The Earthquake forced rapid and huge energy from the earth causing energy transfer from the lithosphere to the ionosphere. Earth plate movements will generate acoustic gravity waves (AGW) in the atmosphere²¹. This wave propagates from the epicenter horizontally and upward into the upper atmosphere at infrasonic speed¹¹⁻¹⁵. This will cause the variation of the plasma in the E- and F-layers which produces the change in the geomagnetic field, H in the E-layer and TEC in the F-layer in the ionosphere^{10,20}.

The geomagnetic responses during large earthquakes have also been previously investigated. Iyemori *et al.*²² observed a short-period magnetic oscillation with period of 3.6 min, about 12 min after the large 2004 Sumatran earthquake near the vicinity of the epicenter. Using an ocean-bottom electro-magnetometer emplaced near the Japan trench, Ichihara *et al.*² observed an impulsive Tsunami induced geomagnetic field variation of the short-duration of about 4-5 min at about 1 min after the main shock and the long-period wave during the 2011 Tohoku earthquake. There was 15 nT geomagnetic variation which corresponded with 2.3 m of sea level change. The observed geomagnetic variations supported by sea-level gauge data indicated that the Tsunami source was determined along the Japan trench at about 100 km from the main rupture zone of the main shock and had a narrow width.

Although the ionospheric GPS TEC and geomagnetic field disturbance during the Tohoku earthquake have been previously investigated^{9,23,24}, the effects have been discussed separately. This paper attempts to investigate the relationship between the ionospheric and geomagnetic responses during the event and suggest the physical mechanisms involved. In this study, ground-based GPS-TEC data over Japan as well as a geomagnetic field measurements from magnetometers located near and far from the epicenter were utilized. The Tohoku earthquake occurred on 11 March 2011 at 05:46:24 UTC, which at 13:46:24 LT with a magnitude of 9.0. It occurred at geographic coordinate of (38.297 ° N, 142.372 ° E) near the east coast of Honshu, Japan with shallow earthquake depth that estimated at 32 km as reported by USGS. Figure 1 shows the locations of the earthquake's epicenter (star), the GPS (dot) and magnetometer (triangle) stations of the GEONET (diamond) and MAGDAS (triangle) networks, respectively.

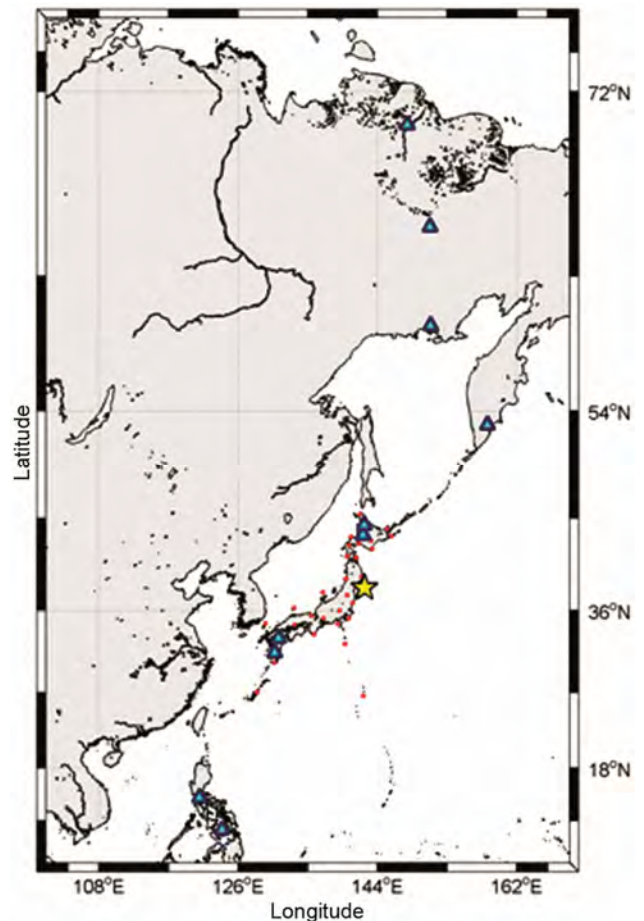


Fig. 1 – The locations of the Tohoku earthquake epicenter (star), GPS (dot) and magnetometer (triangle) stations of the GEONET and MAGDAS networks, respectively

2 Observation of Geomagnetic and Solar Condition

TEC variations in the ionosphere are strongly influenced by regular variation, long-term variation and short-term variations. Long-term variation is influenced by diurnal, seasonal and solar cycle while most of the short-term variations are due to geomagnetic storm and ionospheric disturbance²⁵ which occurs from 0.2 min to 1 h. The measurements of ionospheric disturbance that came from the ground can be disturbed by the strong solar and geomagnetic activities. It is necessary therefore to determine whether the earthquake occurred during low or high solar and geomagnetic conditions.

In order to investigate the geomagnetic and solar activities' influence on VTEC during the earthquake event, geomagnetic and solar data were obtained from WDC (<http://swdcwww.kugi.kyoto-u.ac.jp>) and NOAA (<http://www.swpc.noaa.gov>) during the time of the event and the day after. Figure 2 presents the geomagnetic (Dst, AE, Kp) and solar indices (SSN and F10.7) during the occurrence of the main shock and the day after the Tohoku earthquake from 11-12 March 2011. During the time of the 11 March 2011 earthquake, the geomagnetic values of Dst, AE, and Kp were -80 nT, 638 and 4, respectively, and the geomagnetic activity on that day was classified as “quiet to active” as reported by IPS (<http://www.ips.gov.au>) SSN and F10.7 were 123 and 105, respectively, which showed high solar activity (<http://www.sws.bom.gov.au>). On 12 March, the geomagnetic activity was “quiet to unsettled” with Dst and AE mean values of -34, 248, respectively and Kp sum of 21+. SSN and F10.7 were 121 and 78, respectively, and solar activity was classified as “moderate”.

3 Data Processing and Measurement Technique

The ionospheric disturbances during the 2011 Tohoku earthquake were investigated by using both GPS TEC and magnetometer techniques. GPS data were obtained from the GPS earth observation network (GEONET) in Japan. GEONET consists of more than 1200 dual frequency GPS stations all over Japan (<http://terras.gsi.go.jp/>). This dense, continuous network is an efficient technique to monitor small-scale perturbations⁷. The GEONET data include the carrier-phase and group delays in dual frequency bands ($f_1=1.5754$ and $f_2=1.227$ GHz) at 30 sec intervals. In this analysis, data from 35 GEONET stations covering the entire Japan were collected to investigate the ionospheric disturbances during the

2011 Tohoku earthquake which is enough to plot the VTEC map and show the variation of the VTEC through out the entire Japan. Table 1 shows the list of the GPS stations with their coordinate and distance from the epicenter.

TEC from GPS can be derived using both differential carrier-phase and differential group delay methods. The TEC measurements can be easily obtained using the differential group delay method, but these measurements are prone to

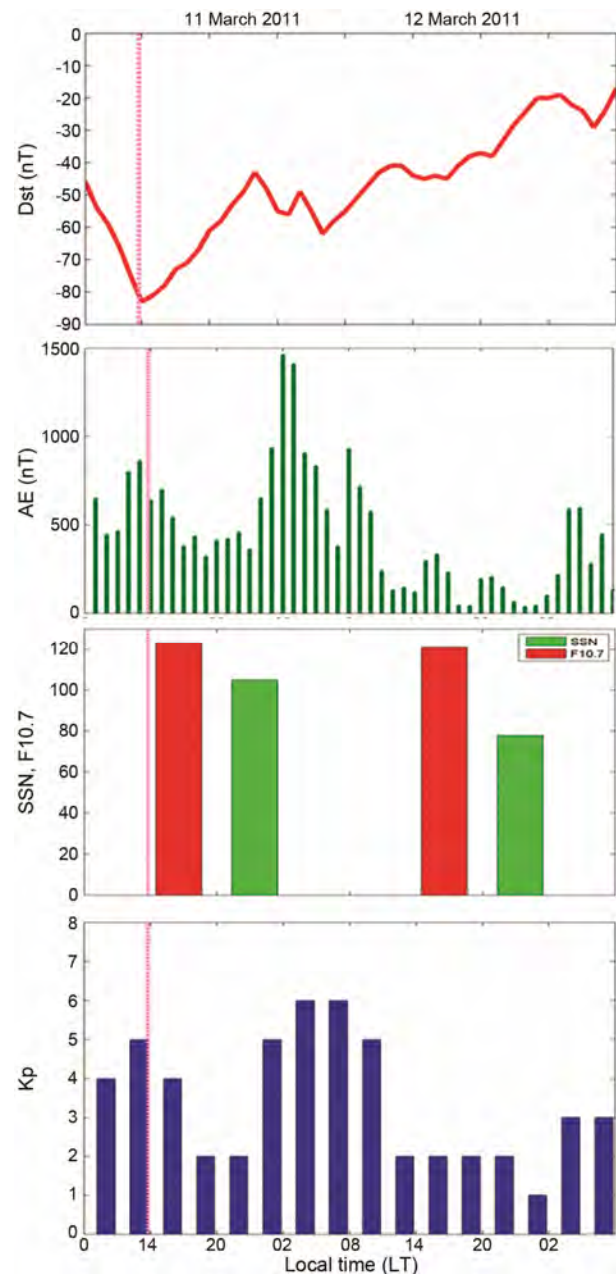


Fig. 2 – Geomagnetic and solar indices for 11 and 12 March 2011. The dotted vertical line indicates the time of the earthquake event

Table 1 – GPS stations of the GEONET network over Japan, their coordinate and distance from the epicenter

Station code	Station location	Geog. coordinate		Distance from epicenter (km)
		(°N)	(°E)	
05500710	Oshika	38.3012	141.5008	76
01670710	Yamada	39.4581	141.9553	134
02020710	Inawashira1	37.5669	140.0727	217
02140710	Kitaibaraki	36.8003	140.7539	219
01910710	Kisakata	39.2061	139.9077	236
00240710	Mutsu	41.3008	141.2133	348
02230710	Chichibu	35.9869	139.0757	389
30410710	Katsura	35.1659	140.2680	395
00230710	Matsumae	41.4664	140.0407	404
05320710	Erimo2	42.1256	143.3157	433
02520710	Hekurajima	37.8505	136.9193	479
01360710	Tomakomai	42.6555	141.6023	489
01400710	Oshamanbe	42.4944	140.3542	497
30860710	Minamizu2	34.6100	138.8384	517
05210710	Obihiro	42.9389	143.1706	520
06300710	Nagoya	35.1684	136.9658	594
05080710	Asahikawa	43.7385	142.4096	605
06020710	Aogashima	32.4635	139.7646	690
06410710	Maizuru	35.4822	135.4158	693
00700710	Kushimoto	33.4834	135.7644	800
03820710	Goka	36.2853	133.2399	837
07670710	Hirosima Fukuyama	34.4504	133.2881	918
07090710	Ooita	33.2284	131.5795	1124
04560710	Kamitsushima	34.6556	129.4821	1220
04690710	Kumamoto Sagara	32.2387	130.8026	1246
06030710	Hahajima	26.6352	142.1628	1297
04930710	Kamiyaku1	30.3817	130.6384	1389
07320710	Kikai2	28.2940	129.9217	1602

multipath resulting in an error worse than 10^{15} m^{-2} . On the other hand, the TEC measurements obtained using the carrier phase method is smoother and precise as compared to the one of group delay but with some level of ambiguity in the initial value of TEC²⁶.

In this analysis, the receiver independent exchange format (RINEX) data from GEONET was processed by using GPS Toolkit (GPSTk) scientific software. GPSTk is developed to read and write, particularly in RINEX format, process and manipulate GPS data. This program is produced by the space and geophysics laboratory, (SGL) of applied research laboratories. The university of Texas at Austin (<http://www.gpsstk.org>). In this study, GPSTk was used to calculate precise VTEC from GPS measurements using the carrier phase method that is

accomplished by correction and removal of carrier phase discontinuity and phase ambiguity. Cycle slips and satellite biases were also removed in order to obtain the absolute VTEC measurements. GPSTk software uses mapping function known as a single layer model to get the VTEC from slant TEC (STEC). This model assumes all the free electron are contain at an altitude of h_m which are 350, 400 and 450 km, which is approximately the altitude of the maximum electron density^{27,28}. The VTEC is determined at the ionospheric pierce point (IPP), which is the altitude of the intersection of the user line-of-sight to the tracked satellite with the center of ionospheric slab. In this work the IPP altitude is set at the altitude of 450 km above the earth surface²⁸.

To investigate the ionospheric response to the 2011 Tohoku earthquake event, VTEC measurements from individual satellite passing were analyzed to observe which among them were the most affected by the seismic activity. These VTEC measurements were examined during the period of the earthquake occurrence up to 4 h following the event. Since the VTEC variations are strongly influenced by its regular variations such as diurnal, seasonal and solar cycle variation, it is necessary to obtain the VTEC that purely affected by the earthquake disturbance by doing a process called de-trending²⁵. Detrending can be done in several ways as it has been done by several researchers, for example by band-pass filter²¹ and high-pass filter²⁵. In this work, The VTEC measurements along individual satellites were smoothed by using the Savitzky-Golay filtering method, with a second order polynomial over a period of 30 min. To obtain the VTEC disturbances caused by earthquake, the VTEC was de-trended by subtracting the filtered VTEC from the original VTEC as illustrated in Fig. 3. A threshold value, marked by the horizontal line in Fig. 3 was set to permit detrended VTEC values with fluctuation amplitude greater than ± 0.07 TECU. Only the VTEC fluctuations above the threshold value were considered as earthquake related VTEC disturbances.

In order to investigate the magnetic disturbances, magnetometer data were obtained from ten magnetometer stations of the MAGnetic Data Acquisition (MAGDAS) network located near and far from the earthquake epicenter along the longitude as shown in Fig. 1. These data were obtained with the sampling rate of one second interval. Table 2 shows the magnetometer stations of the MAGDAS network with their coordinate and distance from the epicenter. To investigate the geomagnetic response to the earthquake, the H

component geomagnetic field was de-trended using the same method as previously used for VTEC.

4 Results and Discussion

The GPS VTEC measurements from all the satellites visible between 13:00-16:00 LT were examined. Based on this observation, only 15 stations with the nearest distance from the epicenter detected significant disturbances. However, all satellites for all stations were taken into consideration for the VTEC mapping. The detailed analysis of these 13 stations is discussed further in section 4.2. Meanwhile, the H-component geomagnetic fields from 10 stations located near and far from the epicenter were also analyzed to investigate for geomagnetic disturbances.

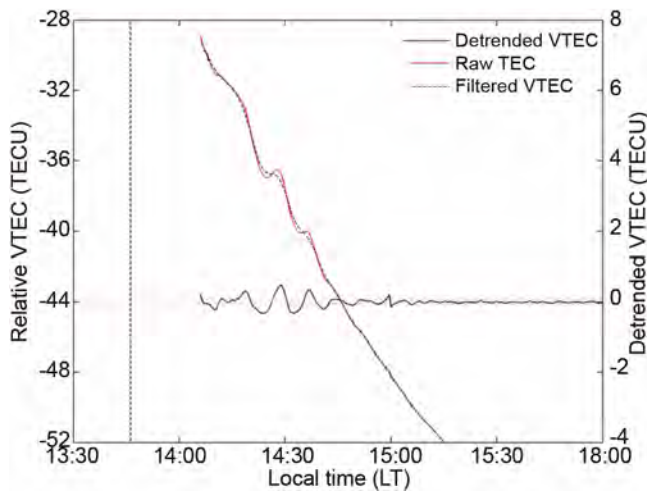


Fig. 3 – The locations of the Tohoku earthquake epicenter (star), GPS (dot) and magnetometer (triangle) stations of the GEONET and MAGDAS networks, respectively

Table 2 – Magnetometer stations of the MAGDAS network with their coordinate and distance from the epicenter

Station code	Station location	Geog. coordinate		Distance from epicenter (km)
		(°N)	(°E)	
ASB	Ashibetsu, Japan	43.46	142.17	575
MSR	Moshiiri, Japan	44.37	142.27	676
KUJ	Kuju, Japan	33.06	131.23	1158
KAG	Kagoshima, Japan	31.48	130.72	1300
PTK	Paratunka, Russia	52.94	158.25	2037
MGD	Magadan, Russia	59.97	150.86	2485
ZYK	Zyryanka, Russia	65.75	150.78	3101
MUT	Muntinlupa, Philippines	14.37	121.02	3385
CEB	Cebu, Philippines	10.36	123.91	3607
CHD	Chokurdakh, Russia	70.62	147.89	3610

4.1 Analysis of the ionospheric TEC variations

In order to ensure that the observed VTEC disturbances were not caused by the geomagnetic and solar activity, VTEC for the day before and after the main shock were also examined. Although not shown in this analysis, VTEC measurements for the day before and after the main shock did not show any significant perturbation⁹. Hence, only co-seismic perturbations related to the 11 March earthquake are highlighted in this paper. During the observation period, ten satellites (PRN4, PRN5, PRN9, PRN12, PRN15, PRN18, PRN21, PRN22, PRN26, PRN27) were visible at 35 stations, but only six (PRN9, PRN15, PRN18, PRN21, PRN26, PRN27) of them showed the significant features of VTEC oscillations. From the 35 stations observed, only measurements from 15 closest stations to the epicenter exceeded the threshold value (± 0.07 TECU) of VTEC disturbance, while the rest lie below the threshold value and thus were not considered for the detailed analysis.

Figure 4 shows the detrended GPS TEC for six detected PRNs at station 0202, which one of the closest station to the earthquake epicenter, viewed from 13:00 to 15:30 LT. Significant VTEC oscillations were observed in both short and long periods about a few minutes after the event. PRN18 shows long period disturbance while the remaining PRNs showed short period disturbance. These could be observed in the form of W and N shaped waves which represent the tsunami and the acoustic waves¹⁰, respectively, as defined in section one. At about 13:54 LT, a series of sudden enhancement-depletion of VTEC can be observed

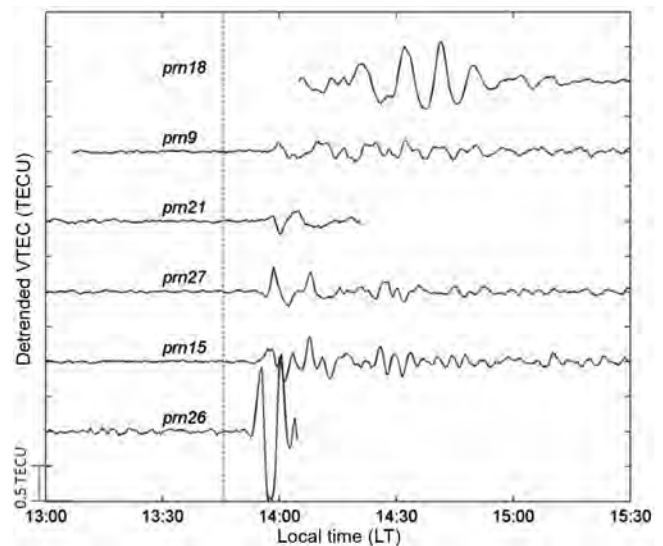


Fig. 4 – Geomagnetic and solar indices for 11 and 12 March 2011. The dotted vertical line indicates the time of the earthquake event

around 7 min after the onset of the earthquake as illustrated in Fig. 4. These VTEC oscillations had a period of 4-6 min.

Figure 5 shows the detrended VTEC of short period disturbance from PRN26 which included 12 nearest stations to the epicenter as example to show the variation of the wave. While another effected PRNs also show their wave variation according to their distance from the epicenter. The figure also shows the distance of the stations to the epicenter which are arranged ascendingly. As shown in the figure, the six nearest station which are 0550, 0167, 0202, 0214, 0191 and 0154 show 'N-type' of wave and the other which are 0024, 0223, 0023, 0532, 0136 and 0140 show the inverted 'N-type' wave disturbance. Oscillation was firstly observed at the nearest station at 7 min and it increased up to 14 min for another station as the station was further away from the epicenter. It is noted that the time lag peak disturbance for the first station was 13 min after the event, and it increased up to 17 min for the stations further away which is in agreement with Tsugawa *et al.*²⁶ observation. The oscillation period was 2-7 min and ended after 38 min which is in close agreement with previous observations^{27,28}. The amplitude decreased and the wavelength tends to become wider as the wave moved further from the epicenter as agreed by Shingawa *et al.*²⁰. This direct acoustic wave is detected in 'N-type' wave type for the station near to the epicenter and inverted 'N-type' for station farther from the epicenter¹⁰. Figure 6

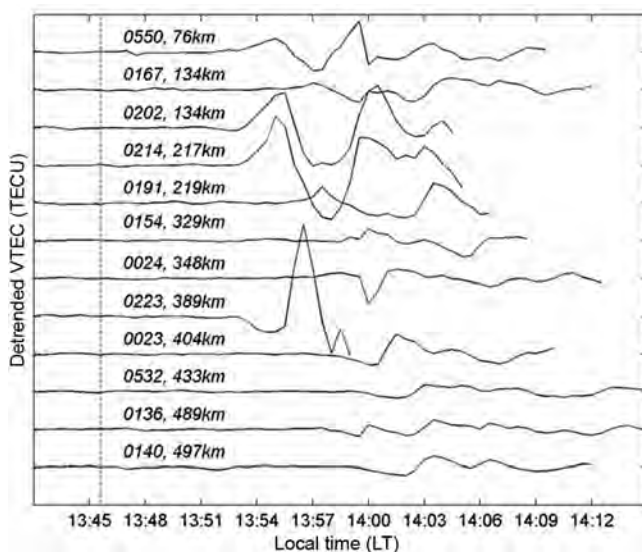


Fig. 5 – VTEC detrending for long wave of PRN18 at station 0550. The vertical dotted line indicates the time of the event and the horizontal dotted lines is the threshold of the detrended VTEC. The time of main shock is at 13:46:24 LT

Figure 6 shows the detrended VTEC of the long period wave observed by PRN 18 which was detected as long-wave or Tsunami-wave at the 15 stations nearest to the epicenter. These stations were arranged from the nearest to the farthest from the epicenter. The start time of the disturbances increased as the distance of the station increased. As the stations' distance increased, the wave period got wider, the disturbance duration also became longer and the amplitudes decreased. The effect of the disturbance lasted at station 3086 which is 517.6 km from the epicenter. The VTEC oscillation of PRN18 was firstly observed at the nearest station, 0550 about 20 min after the main shock at 14:06 LT where the time lag of peak disturbance was 42 min. This wave had a period of 10 min and duration of 60 min. The other stations observed showed that the time the oscillations started varied from 27 min to 1 h where the time increased as the stations' distance from the epicenter increased and the same applied to the time lag. This characteristic is in close agreement with previous study^{17,30} which conducted a study on the same earthquake, as well as with the study during the 2001 Peru earthquake⁷. The wavelength of this type of wave was also longer with lower amplitude and it weakened with time^{20,30}.

Figure 7 shows the location of GPS stations with the IPP of peak disturbance of PRN 26 and PRN 18. The IPP of PRN 26 all located northeast from the epicenter while the IPP of the PRN 18 located from southwest to northwest from the epicenter. The nearest IPP station which is 0223 showed the fastest and most significant impact of disturbance

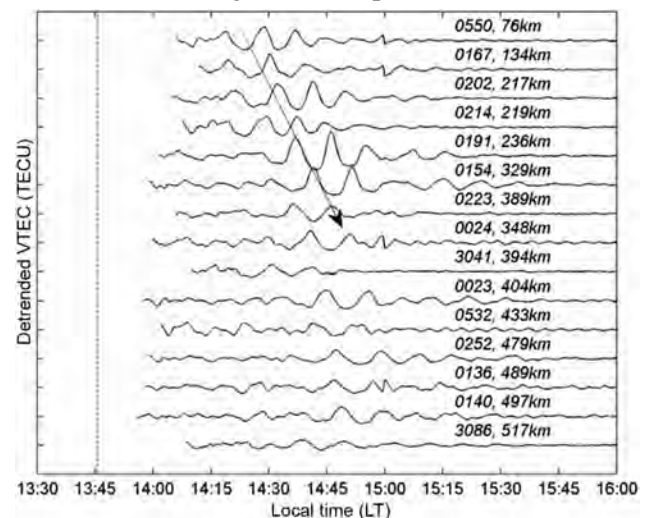


Fig. 6 – Detrended VTEC for PRN18 for 15 nearest stations from the epicenter

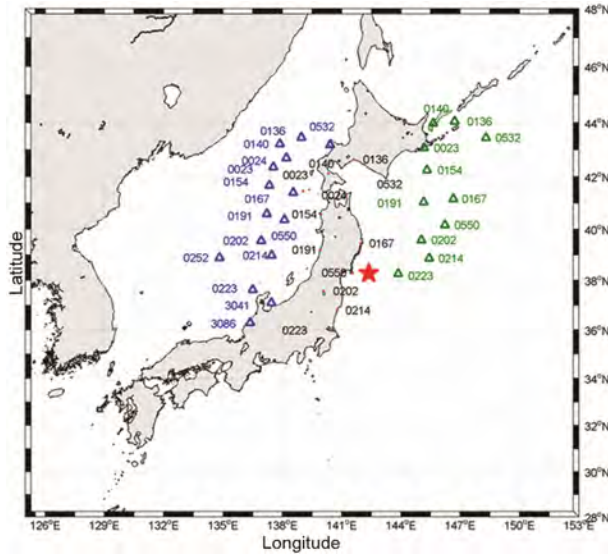


Fig. 7 – Map of IPP for PRN 18 (blue triangle) and PRN 26 (green triangle). The black dots are the GEONET station and the red star indicates the epicenter of the earthquake

with the highest amplitude of VTEC increased reached 2 TECU at 13:57 LT. The oscillation began to occur at 7 min from the main shock with a time lag of 11 min. This wave may be derived from Rayleigh wave which has a higher velocity and reach the ionosphere quickly. The large amplitude proved that strong vertical ground displacement due to the earthquake occurred along the fault⁹. This was followed by other closer IPP stations, 0214, 0202 and 0550 which increased about 1 TECU. IPP distance closer to the epicenter will be more affected than the IPP stations of greater distances from the epicenter³². Kamogawa¹⁵ observed a localized seismo-tsunamigenic hole, which appeared as a wide sudden depression triggered by the co-seismic surface motion, Rayleigh wave travelling, and Tsunami wave travelling. The depression appeared after initial enhancement of a 4 min period and disappeared within 40 min. However, that depression was not shown in our observation. The entire wave came back to a normal state after approximately 30 min.

Observation was made on the location of the IPP of each of the 15 stations of PRN18 to predict the directivity of the propagation. From the observation, the IPP for these 15 stations are located from the southwest to the northwest of the epicenter as shown in the Fig. 5. Three IPPs located at the south had a lower amplitude (0.1 TECU) than the IPPs in the northern part with enhancement of 0.9 TECU even though the IPPs in the south are closer to the epicenter

compared to the IPPs in the north. The value of this enhancement decreases with the increase of distance from the epicenter. This finding is in agreement with another study which came to the same observation when conducting case studies on the same earthquake^{2,9,14}. This finding was also observed during the 2004 Sumatra Andaman earthquake, where the TEC enhancement for the sub-ionospheric points located in the northern part was higher while the TEC enhancement of the sub-ionospheric point located in the southern part was smaller^{12,20}.

The horizontal velocity of propagation was calculated only for selected IPP stations which are located in the same direction. The distance between the IPP was divided by the difference in time between the time lag of peak arrivals. Table 3 shows the summary of the calculation of velocity, period and the duration of the oscillation of certain stations. The velocity of the short wave ionospheric disturbances varied from 894 m/s, 1210 m/s and 2862 m/s with average propagation velocity of ionospheric disturbance of 1655 m/s. The velocity of the long-wave disturbance was smaller where the average propagation velocity was 226 m/s. There were three types of waves observed from the range of velocity. The first type of wave with velocity of about 1000 m/s is classified as acoustic wave that was induced by the sudden uplift from the sea surface when acoustic wave was interacting in the atmosphere. This wave is similar to sound velocity at ionospheric height^{8,13,36}. The second wave is recognized as Rayleigh wave which propagated with velocity of ~2000-3000m/s. The first peak of the disturbance may be caused by acoustic wave generated by Rayleigh wave. The third type of wave with velocity of 200-250 m/s indicate of tsunami wave. This type of wave corresponds to the gravity mode of atmospheric co-seismic wave³⁵. These three types of waves were also observed by previous studies using the GPS VTEC technique^{15,19,37}, and ionosonde technique^{17,18}. Similar observations were also seen through previous studies on the 2003 Tokachi Oki earthquake⁴, the 2004 Sumatra Andaman fault¹¹ and the 2005 Sumatran earthquake¹³.

In this study, it is concluded that the directivity of the wave propagation after the earthquake is northward. Hasbi¹³ reported that only two stations in the northeast showed TEC enhancement while the stations located in the south and east did not show any enhancement in the 2005 Sumatran earthquake. The directivity of the TEC variations with respect to the

Table 3 – Short and long period ionospheric and magnetic field disturbance parameters for the nearest stations

Wave type	Station	T _{peak} (UT)	Latitude (°N)	Longitude (°E)	Time lag δt (s)	ΔD (km)	ΔT (s)	Period (s)	Duration (s)	Velocity (m/s)	Average velocity (m/s)
Ionospheric parameters											
Short period	0223	5.942	38.265	143.851	608.40	161.00	180	210	360	894	1655
	0214	5.992	38.862	145.538	788.40	91.50	75.60	300	720	1210	
	0202	6.008	39.583	145.026	846.00	515.2	180.00	360	660	2862	
	0136	6.058	44.040	146.724	1026.00			240	1020		
H-component parameters											
	ASB	5:56	43.46	142.17	600			240	240		
	KUJ	5:57	33.06	131.23	660			240	360		
Ionospheric parameters											
Long period	0167	6.500	41.399	138.542	2617	138.4	691	900	1800	200	226
	0154	6.692	41.973	137.063	3308	80.32	209	1020	1680	384	
	0023	6.750	42.682	137.250	3517	78.19	839	720	1560	93	
	0140	6.983	43.224	137.862	4356			900	1440		

azimuth from the epicenter could be caused partially by directivity in the response of the electron density variation to the acoustic waves in the neutral atmosphere¹². Directivity of TEC changes is caused by changes in plasma density due to neutral motion by acoustic waves in the obliquity of geomagnetic field line, assuming the wave is propagated in all directions from a point source. The plasma directivity is propagate perpendicularly with geomagnet field line due to Lorentz force that imposed to the charged particle. This is means in the north hemisphere, magnetic field line block the CID from propagate to the north⁴. However according to Rolland *et al.*¹⁹, due to gravity waveline is horizontal and the CID is longitudinal, the opposite propagation is logic. However according to Astafyeva and Heki¹⁰, CID detected near distance to the epicenter of about 50-150 km yet to perpendicular with geomagnetic field line, so the CID is detected by GPS.

Figure 8 shows the map of detrended VTEC all over Japan. The TEC map was produced by using detrended VTEC for all stations of which its PRN was affected by the earthquake. The VTEC was plotted within a 10 min interval period starting from 13:45 LT to 15:45 LT which involved an observation period of two-hours. There was almost no effect of disturbance in the first 10 min of the earthquake, except for the northeast area, which showed effect 6 min after the time of the event which was observed through signal disturbance from PRN 26 which is short wave disturbance. Significant changes burst in

the second 10 min (13:55-14:05 LT), where the effect of disturbance was shown in almost all the places, especially to the northeast of the epicenter, but less obvious for the place farther from epicenter. At the 14:15 - 14:55 LT, visible effects can be seen in the west and northwest which indicated the long period disturbance from PRN 18. It appeared about 20 min to 1 h after the main shock. Still there was an effect at the time of 14:55 - 15: 45 LT in the southeast, but the effects faded gradually. Previous observation over Japan¹⁵ shows that the direction is southwestward while another observation³⁸ shows that the directivity is northwestward. The dissimilarity in the observation could be due to the directivity factor that plays a major role in determining the characteristics of the ionospheric VTEC disturbance.

4.2 Analysis of geomagnetic field disturbances

Several MAGDAS magnetometer stations were selected from the southwest to the northeast of Japan with a distance of 570 – 3610 km from the epicenter to observe the directivity of the wave propagation. Figure 9 shows the detrended H-component of geomagnetic field for all stations from 13:30-15:00 LT. From the figure, all stations have a global impact with the peak of disturbance at 14:18 LT and 32 min time lag of peak disturbance after the main shock. CHD showed changes at 13:57 LT; however, the period does not correspond to acoustic waves. Only two nearest stations from the epicenter, namely ASB and KUJ which are located north and southwest with

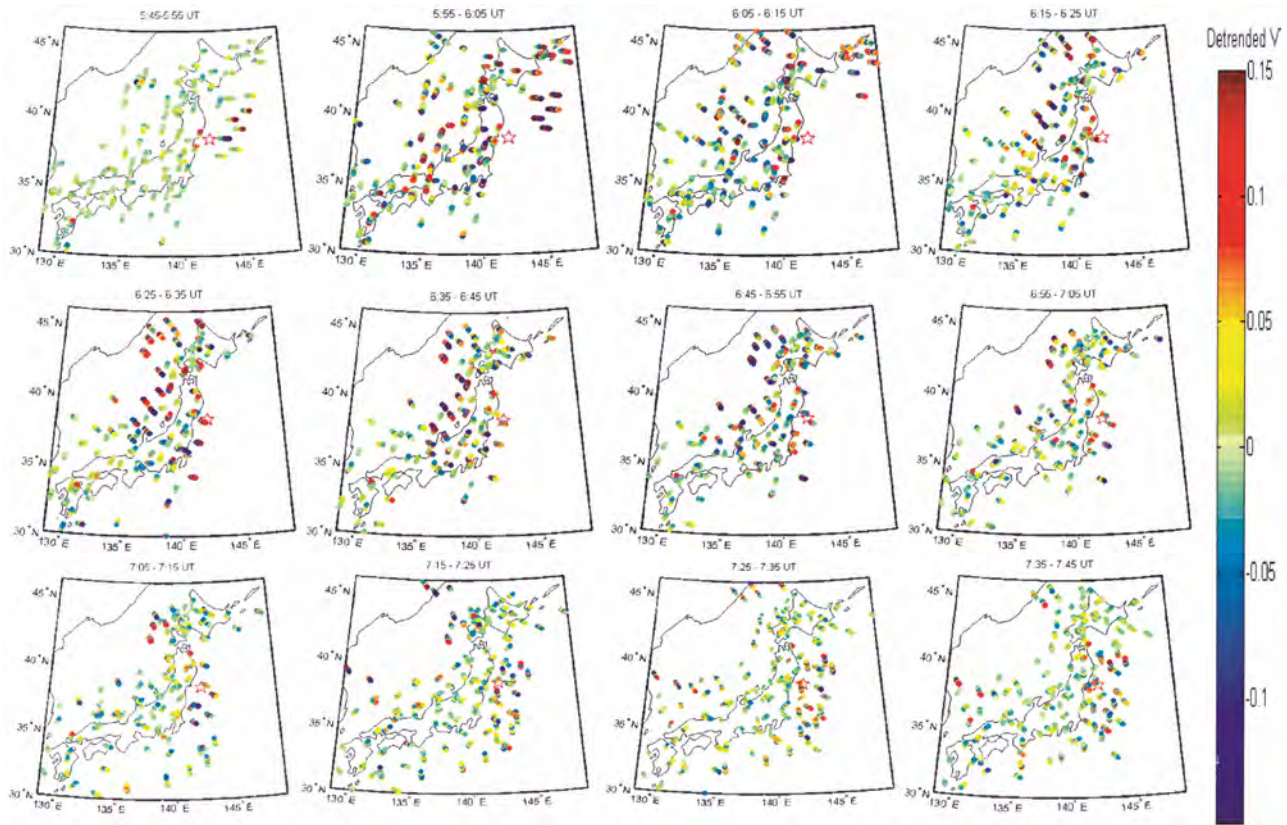


Fig. 8 – VTEC map over Japan from 13:45 LT to 15:45 LT on 11th Mar 2013. The star indicates the epicentre of the earthquake

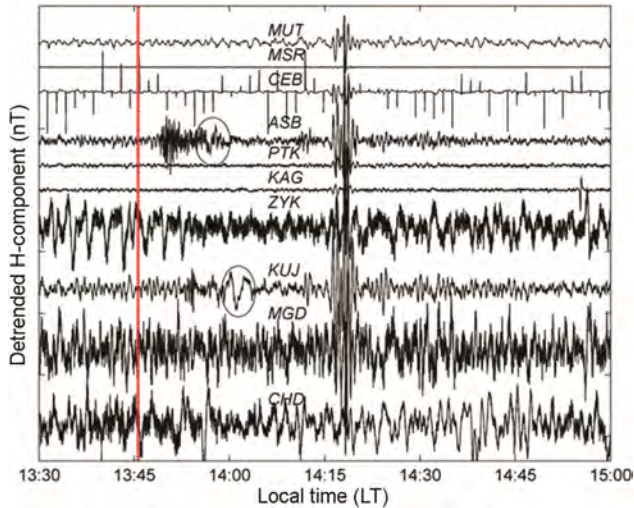


Fig. 9 – Detrended H-component of magnetic field for all observation stations. The vertical dotted line indicates the time of the event. The circle shows the wave that is associated with the event

a distance of 575 km and 676 km from the epicenter respectively that showed significant effects of the Tohoku earthquake.

Figure 10 shows the one second detrended H component of the geomagnetic field from 13:42 to 14:09

LT for ASB and KIJ. The rapid fluctuation at station ASB was observed 3 min after the main shock started from 13:49 to 13:52 LT, and the rapid fluctuation at station KIJ was observed 7 min after the main shock started at 13:53 to 13:55 LT. This sudden fluctuation with small period and amplitude is due to the vibration of the magnetometer device during the earthquake conducted from the seismic wave from the earth crust¹³. This is because the seismic waves caused the earth's crust to conduct. When the earth shakes with velocity v in a magnetic field B of the earth during an earthquake, $v \times B$ electromotive force will be formed in the earth to produce electric current flows in the conducting earth's crust. This current increases the geomagnetic field at the observation station on the earth's surface. As the intensity of the magnetic field of the earth is more than 30,000 nT, detection of small movement in the background magnetic field will cause large variation to the magnetic field detected by sensors¹³.

The actual fluctuation due to the event was firstly observed at the ASB station about 10 min after the earthquake, commencing from 13:56 - 14:00 LT. The actual oscillation was observed at KIJ about 11 min after the event, starting from 13:58 LT to 14:04 LT.

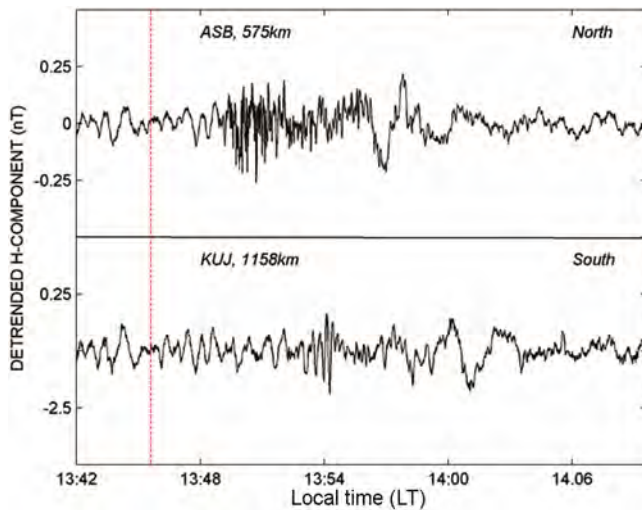


Fig. 10 – Detrended H-component of magnetic field for two nearest stations (ASB and KUU) located north and south from the epicenter

The oscillation period for ASB and KUU stations was 4 min and 6 min and lasted for 15 and 18 min, respectively. Similar observation was also found and they suggested that the observed geomagnetic field changes that started at approximately 13:55-14:00 LT are directly related to the ionospheric disturbance since the occurrence time and the main features of the time variations of TEC and the geomagnetic field were the same²⁴. The time lag of peak disturbance for ASB and KUU stations are 12 min and 14 min, respectively, which is consistent with the time necessary for the acoustic wave to travel from earth to the ionosphere and reflect back to the E-layer to form a duct resonance²². The oscillation period for both the ASB and KUU station is similar which is 4 min. The wave with period of 3-5 min which are induced by the sea surface current are considered to be trapped in the thermal duct in the mesosphere under altitude of 100-120 km and these waves have a standing wave character directly over the earthquake region. Based on numerical simulations with realistic atmospheric parameters and different sources of acoustic waves in the atmosphere, the oscillation wave period of 3-5min tend to appear at the ionospheric E-layer as a result of the energy from the lower atmosphere and this oscillation lasts over a relatively long period²⁰. As shown in Fig. 10, ASB which is located north from the epicenter has higher amplitude of H-component compared to KUU that is located south from the epicenter. It is therefore conclude that the directivity of the wave recorded by the magnetometer is northward.

Iyemori²² suggested the ionospheric dynamo mechanism in the ionospheric E-layer is at the altitude of 100-120km above the epicenter. This mechanism is generated by vertical wind oscillations produced by atmospheric duct resonance from the earthquake. During an earthquake, the vertical movement of the ground causes atmospheric waves to propagate towards the ionosphere as acoustic wave. Some of the acoustic wave is reflected back to the ionospheric E-layer to form a duct resonance. The acoustic wave produce vertical wind with resonance frequency of 3.6 min in the E-region which generates the dynamo current. The change in the magnetic field due to the electric current induced in the sea or by the ionospheric disturbance are assumed to have been caused by the devastating tsunami of the Tohoku event²⁴. When tsunamis occur, the motion of electrically conductive seawater induces an electromotive force in the ambient geomagnetic field due to Faraday's law, which results in secondary electromagnetic (EM) field variations²⁰.

Geomagnetic observations for stations ASB and KUU (Fig. 10) were correlated with co-seismic disturbance observed from the GPS TEC. The peak arrivals of both GPS TEC and geomagnetic disturbance were observed about 12-17 min after the earthquake which shows the consistency in time lag of the ionospheric magnetic disturbance. The earlier magnetic field response to the earthquake is due to the shorter time required by the acoustic wave to propagate to the ionospheric E-layer at altitude 100-120 km measured by the magnetometer than the time required to propagate to the F-layer at altitude 450 km measured by GPS satellites¹³. It also shows the correlation in both the GPS TEC and magnetic field in terms of oscillation period. TEC shows 2-7 min of oscillation period while magnetic field shows 4min oscillation period. Some of the ducted acoustic wave trapped in the E-layer leaks into the thermosphere, producing oscillations with similar periods in the ionospheric F-layer¹³. We found good correlation between the short period of GPS TEC and magnetic pulsation. As per our observation, the enhancement of VTEC and the magnetic field occurred about 4 min to 30 min after the earthquake, which is about 1 hour before the Tsunami, and thus can be used as Tsunami early warning system.

5 Conclusions

This paper investigated the ionospheric and geomagnetic responses during the 11 March 2011 Tohoku earthquake using the GPS-TEC from

GEONET station located in the zone near to the epicenter and geomagnetic field from MAGDAS magnetometer station network located near and far from the epicenter. Three types of waves were observed from GPS-VTEC study, which are the direct acoustic wave that propagated with velocity of ~1000m/s with a period of 2-7 min that oscillated 7-14 min after the earthquake. The second type of wave is the secondary acoustic wave that excited by the Rayleigh surface wave with velocity of ~3000m/s. The third type of wave is the gravity wave from the propagating tsunami with a period of 10-15 min and oscillated 20-45 min after the main shock. We found that the directivity of the wave propagation was northward from the epicenter, similar to those found by other studies. Geomagnetic field study showed that the wave propagated northward since the north station show the higher amplitude compare to the south station. The correlation between the VTEC and geomagnetic field disturbances deduced that the direct acoustic wave generated near the epicenter propagated upwards to the ionosphere and induced disturbance in the ionospheric E and F regions.

Acknowledgment

This research is partly funded by Malaysia Government, Ministry of Education through University Kebangsaan Malaysia (UKM) under the DPP-2014-052 research grant.

References

- 1 Toh H, Satake K, Hamano Y, Fujii Y & Goto T, *J Geophys Res*, 116 (2011) pp 10.
- 2 Ichihara H, Hamano Y, Babab K & Kasaya T, *Earth Planet Sci Lett*, 382 (2013) 117.
- 3 Hasbi A M, Momani M A, Ali M A M & Misran N, 'The relationship between the Ionospheric and Magnetic Disturbances during the 28 March 2005 Sumatran Earthquake', *Icon-Space (Malaysia)*, 2009.
- 4 Heki K & Ping J, *Earth Planet Sci Lett*, 236 (2005) 845.
- 5 Calais E & Bernard J, *Geophys Res Lett*, 22 (1995) 1045.
- 6 Ducic V, Artru J & Lognonne P, *Geophys Res Lett*, 30 (2003) 1.
- 7 Artru J, Ducic V, Kanamori H, Lognonné P & Murakami M, *Geophys J Int*, 160 (2005) 840.
- 8 Heki K, *Geophys Res Lett*, 38 (2011) pp 20.
- 9 Rolland L M, Lognonne P, Astafyeva E & Kherani E A, *Earth Planets Sp*, 63(2011), 853.
- 10 Astafyeva E & Heki K, *Earth Planets Sp*, 61 (2009) 939.
- 11 Heki K, Otsuka Y, Choosakul N, Hemmakorn N, Komolmis T & Maruyama T, *J Geophysical Res*, 111 (2006) B0931.
- 12 Otsuka Y, Kotake N, Tsugawa T, Shiokawa K, Ogawa Effendy T, Saito S, Kawamura M, Maruyama T, Hemmakorn N & Komolmis T, *Earth Planets Sp*, 58 (2006) 159.
- 13 Hasbi A M, Momani M A, Mohd Ali M A, Misran N, Shiokawa K, Otsuka Y & Yumoto K, *J Atmos Solar-Terrestrial Phys*, 71 (2009) 1992.
- 14 Chen C H, Saito A, Lin C H, Liu J Y, Tsai H F, Tsugawa T, Otsuka Y, Nishioka M & Matsumura M, *Earth Planets Sp*, 63 (2011) 881.
- 15 Kamogawa M, Kakinami Y, Watanabe S & Watanabe Y, *Terrestrial Atmos Ocean Sci*, 23 (2012) 327.
- 16 Liu J Y, Tsai Y B, Ma K F, Chen Y I, Tsai H F, Lin C H, Kamogawa M & Lee C P, *J Geophys Res*, 111 (2006) A05303.
- 17 Liu J Y & Sun Y Y, *Earth Planets Sp*, 63 (2011) 897.
- 18 T Maruyama, T Tsugawa, H Kato, M Ishii & M Nishioka, *J Geophys Res Sp Phys*, 117 (2012) 1.
- 19 Rolland L M, Lognonné P & Munekeane H, *J Geophys Res*, 116 (2011) 1.
- 20 Shinagawa H, Iyemori T, Saito S & Maruyama T, *Earth Planets Sp*, 59 (2007) 1015.
- 21 E L Afraimovich, E I Astafyeva & V V Kirushkin, *Int J Geomagn Aeron*, 6 (2005) GI2002.
- 22 T Iyemori, M Nose, D Han, Y Gao, M Hashizume, N Choosakul, H Shinagawa, Y Tanaka, M Utsugi, A Saito, H McCreadie, Y Odagi & F Yang, *Geophys Res Lett*, 32 (2005) L20807.
- 23 Saito A, Tsugawa T, Otsuka Y, Nishioka M, Iyemori T & Matsumura M, *Earth, Planets Sp*, 63 (2011) 863.
- 24 Utada H, Shimizu H, Ogawa T, Maeda T, Furumura T, Yamamoto T, Yamazaki N & Yoshitake Y, *Earth Planet Sci Lett*, 311 (2011) 11.
- 25 Husin A, Abdullah M & Momani M A, *Radio Sci*, 46 (2011) pp 10.
- 26 Komjathy A, Galvan D A, Stephens P, Butala M D, Akopian V, Wilson B, Verkhoglyadova O, Mannucci A J & Hickey M, *Earth Planets Sp*, 64 (2012) 1287.
- 27 Hasbi A M, *Analysis of ionospheric disturbances before and during earthquake over sumatra*. Fakultas Kejuruteraan dan Alam Bina, Universiti Kebangsaan Malaysia, 2011.
- 28 Liu J, Chen R, Kuusniemi H, Wang Z, Zhang H & Yang J, *J Glob Position Syst*, 9 (2010) 22.
- 29 Warnant R & Pottiaux E, *Earth Planets Sp*, 52 (2000) 1055.
- 30 Maeda T, Furumura T, Sakai S & Shinohara M, *Earth Planets Sp*, 63 (2011) 803.
- 31 Tsugawa T, Saito A, Otsuka Y, Nishioka M, Maruyama T, Kato H, Nagatsuma T & Murata K T, *Earth Planets Sp*, 63(2011) 875.
- 32 Calais E & Minster B, *Phys Earth Planet Inter*, 105 (1998) 167.
- 33 Tsugawa T, Saito A, Otsuka Y, Nishioka M, Maruyama T, Kato H, Nagatsuma T & Murata K T, *Earth Planets Sp*, 63 (2011) 875.
- 34 Makela J J, Lognonné P, Hébert H, Gehrels T, Rolland L, Allgeyer S, Kherani A, Occhipinti G, Astafyeva E, Cosson P, Loevenbruck A, Clévéde E, Kelley M C & Lamouroux J, *Geophys Res Lett*, 38 (2011) 13.
- 35 Matsumura M, Saito A, Iyemori T, Shinagawa H, Tsugawa T, Otsuka Y, Nishioka M & Chen C H, *Earth Planets Sp*, (2011) 885.
- 36 Lognonné P, Artru J, Garcia R, Crespon F, Ducic V, Jeansou E, Occhipinti G, Helbert J, Moreaux G & Godet P E, *Planets Space Sci*, 54 (2006) 528.
- 37 Tsai H, Liu J, Lin C & Chen C, *Earth Planets Sp*, 63 (2011) 859.
- 38 Toh H, Satake K, Hamano Y, Fujii Y & Goto T, *J Geophys Res Solid Earth*, 116 (2011) 1.